LETTERS
https://doi.org/10.1038/s41567-020-01137-4

nature physics

Maximum information states for coherent scattering measurements

Dorian Bouchet[1,3]✉, Stefan Rotter[2] and Allard P. Mosk[1]

The use of coherent light for precision measurements has been a key driving force for numerous research directions, ranging from biomedical optics[1,2] to semiconductor manufacturing[3]. Recent work demonstrates that the precision of such measurements can be substantially improved by tailoring the spatial profile of light fields used for estimating an observable system parameter[4–10]. These advances naturally raise the intriguing question of which states of light can provide the ultimate measurement precision[11]. Here we introduce a general approach to determine the optimal coherent states of light for estimating any given parameter, regardless of the complexity of the system. Our analysis reveals that the light fields delivering the ultimate measurement precision are eigenstates of a Hermitian operator that quantifies the Fisher information from the system's scattering matrix[12]. To illustrate this concept, we experimentally show that these maximum information states can probe the phase or the position of an object that is hidden by a disordered medium with a precision improved by an order of magnitude compared with unoptimized states. Our results enable optimally precise measurements in arbitrarily complex systems, thus establishing a new benchmark for metrology and imaging applications[3,13].

No physical observable can be determined with absolute certainty. Instead, the noise inherent in any measurement process sets a fundamental limit on the precision that a physical observable can be estimated with[11,14]. Whenever light or other kinds of electromagnetic radiation are involved in a measurement, a necessary condition to reach this ultimate precision is the optimization of the spatial distribution of the radiation field in the measured system[13]. To achieve this goal, a crucial task is to identify the spatial pattern that should be imprinted on the incoming field to get the maximum information out of it. First progress in this direction has recently been made using wavefront shaping techniques and metasurfaces to precisely estimate lateral displacements[4,8], fluorophore positions[5,6], spectral shifts[7] or phase variations[9].

A central challenge that remains unresolved, however, is identifying a unifying approach to reach the ultimate precision limit that is applicable even to complex scattering systems. Earlier work suggests that such an approach should be connected to the concept of Fisher information[5,10,11,14], which quantifies the amount of information relevant to the estimation of a given parameter from measured data. However, for the generic case of a complex medium, the Fisher information is intrinsically linked to the microstructure of the medium[10], which is not only overwhelmingly complex in realistic systems but also typically unknown.

Here, we overcome this difficulty by expressing the Fisher information in terms of a Hermitian operator that depends on the system's optical scattering matrix. Based on this idea, we introduce and experimentally demonstrate a direct approach to generate optimal coherent states of light for parameter estimation. These light states are shown to be specifically tailored even to a complex system, not only with respect to the specific observable of interest, but also with respect to the position of the observer. By unambiguously identifying these optimal light states, we establish a new general benchmark for metrology and imaging applications[3,13]. Furthermore, in the ideal case for which all optical modes supported by the system are accessible to the observer, our analysis reveals that maximum information states are, at the same time, the optimal states for optical micromanipulation[15,16], thereby uncovering a fundamental relationship between information theory and measurement backaction.

To set up this approach, we recall that a measurement scheme is optimal when the measurements, the estimation function and the choice of the incident state are all optimal concurrently[11]. To realize this situation for coherent states of light, we start with a general model of scattering measurements on a complex medium parameterized by a scalar parameter θ (Fig. 1). This parameter can be a global parameter characterizing the entire scattering medium. It can also be a local parameter of limited spatial extent, such as the phase or the position of a small phase object hidden behind a scattering material, as in our experiments. We illuminate the medium from the far field by an incident coherent state $|E^{\mathrm{in}}\rangle$ characterized by the coefficients $\{E_1^{\mathrm{in}}, \ldots, E_M^{\mathrm{in}}\}$ in M spatial modes, which are individually addressed using wavefront shaping techniques[17]. The far field of the outgoing coherent state $|E^{\mathrm{out}}\rangle$ is then characterized by the coefficients $\{E_1^{\mathrm{out}}, \ldots, E_N^{\mathrm{out}}\}$ in N spatial modes using a homodyne detection scheme, which introduces an external reference beam and measures the resulting number of photons in each spatial mode. The number of outgoing spatial modes can be taken as low as $N=1$, a feature that can be relevant for applications requiring a fast single-channel detector.

Noise fluctuations in the measured data fundamentally limit the achievable precision on the determination of θ. This limit is mathematically expressed by the Cramér–Rao inequality, which sets a lower bound on the variance of unbiased estimators of θ. In general, the Cramér–Rao bound is given by the reciprocal of the Fisher information $\mathcal{J}(\theta) = \mathbb{E}\left([\partial_\theta \ln p(X;\theta)]^2\right)$ where X is an N-dimensional random variable representing the data, $p(X;\theta)$ is a joint probability density function and $\mathbb{E}$ denotes the expectation operator acting over noise fluctuations[14]. Here, we assume that this noise arises only from the quantum fluctuations of coherent states, and not from other possible noise sources such as sample-to-sample or wave-to-wave fluctuations[18]. Considering that noise fluctuations are statistically independent for any two different outgoing modes,

[1]Debye Institute for Nanomaterials Science and Center for Extreme Matter and Emergent Phenomena, Utrecht University, Utrecht, the Netherlands. [2]Institute for Theoretical Physics, Vienna University of Technology (TU Wien), Vienna, Austria. [3]Present address: Université Grenoble Alpes, CNRS, LIPhy, Grenoble, France. ✉e-mail: dorian.bouchet@univ-grenoble-alpes.fr

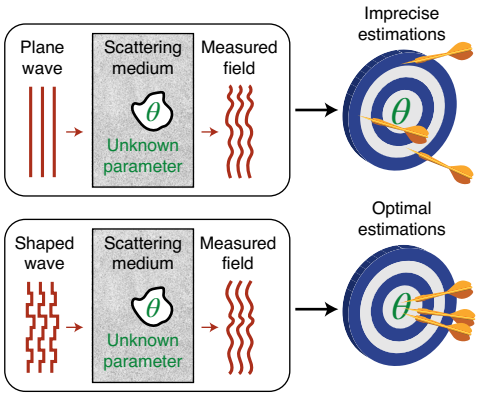

Fig. 1 | Principle of an optimal coherent scattering measurement. A scattering medium is characterized by an unknown parameter θ. This parameter is estimated by illuminating the medium with coherent light and by measuring the outgoing field state via a homodyne detection scheme. In many cases, plane wave illumination leads to imprecise estimations (top). The optimal incident states we generate here using wavefront shaping techniques enable the best estimations possible (bottom).

we derived the following simplified expression for the Fisher information (Supplementary Section 1.1):

$$\mathcal{J}(\theta) = 4\sum_{k=1}^{N} \left|\partial_\theta E_k^{\text{out}}\right|^2 . \qquad (1)$$

This expression is obtained by considering a specific homodyne detection scheme, composed of a high-intensity reference beam that interferes with the kth spatial mode with a phase $\phi_k = \arg(\partial_\theta E_k^{\text{out}})$. Alternatively, one can also calculate the quantum Fisher information $\mathcal{I}(\theta)$, which sets a more general bound on the variance of unbiased estimators holding for any positive-operator-valued measure[19]. When evaluating the quantum Fisher information for an N-mode coherent state composed of simply separable pure states, we find that it coincides with equation (1) so that $\mathcal{I}(\theta) = \mathcal{J}(\theta)$ (Supplementary Section 1.2), thereby demonstrating that the homodyne detection scheme considered here is optimal for the estimation of θ.

We consider an incident state $|E^{\text{in}}\rangle$ as being optimal for the Fisher information it generates when the corresponding outgoing state $|E^{\text{out}}\rangle$ maximizes equation (1) for a given number of incident photons. To identify this state, the pivotal quantity is the scattering matrix S of the medium[12], which relates incoming and outgoing states via $|E^{\text{out}}\rangle = S|E^{\text{in}}\rangle$. Using this relationship, the Fisher information can be written in the quadratic form $\mathcal{J}(\theta) = 4\langle E^{\text{in}}|F_\theta|E^{\text{in}}\rangle$, where we used bra–ket notations for the complex inner product. We designate the term F_θ in the centre of this expression as the Fisher information operator that takes on the remarkably simple form (Supplementary Section 1.3)

$$F_\theta = (\partial_\theta S)^\dagger \partial_\theta S , \qquad (2)$$

where † stands for the conjugate transpose. As this operator F_θ is Hermitian by construction, the incident state that maximizes the Fisher information is given by the eigenstate associated with the largest eigenvalue of F_θ. Furthermore, in the limit of small parameter variations, we obtained a closed-form expression of the minimum-variance unbiased estimator (Supplementary Section 1.4), which is the optimal estimation function. Importantly, the variance of this estimator always reaches the Cramér–Rao bound, even for small numbers of incident photons. This confirms that the Fisher information is here the relevant quantity to assess the precision achievable with different light states.

To demonstrate how to generate these maximum information states, we performed proof-of-principle experiments at optical frequencies (at a wavelength of 532 nm). We first choose as the observable parameter θ that we aim to estimate, the phase shift φ generated by a small cross (total length of 48 µm) displayed by a spatial light modulator (SLM), as represented in Fig. 2a. This target is hidden 1.2 mm behind a ground glass diffuser (scattering angle 15°). Our experimental set-up includes a second SLM used to control the phase of the incident field and a detection scheme based on off-axis holography (Extended Data Fig. 1). The experimental procedure starts by measuring three reflection matrices for different values of φ, which allows us to access both the reflection matrix r and its derivative $\partial_\varphi r$ for 2,437 incident states and 2,465 outgoing states (Methods). Despite the large size of the measured reflection matrix, it constitutes only part of the full S matrix of the medium. This is not a limitation of our approach, however, as it also applies to non-unitary and non-square matrices. Defining the operator $f_\varphi = (\partial_\varphi r)^\dagger \partial_\varphi r$, the eigenvector associated with the largest eigenvalue of f_φ is the optimal incident state based on the available knowledge. Illuminating the medium with this state using the input SLM, we measured the spatial distributions of the outgoing signal intensity (Fig. 2b) and of the Fisher information per unit area (Fig. 2c), respectively normalized by the average signal intensity and by the average Fisher information per unit area under plane wave illumination. Averaging over the field of view, the maximum information state generates a 300-fold enhancement of the Fisher information along with a 20-fold intensity enhancement compared with the average values measured under plane wave illumination.

We then explicitly checked how the maximum information state is shaped in the near field of the cross-shaped phase perturbation. To this end, we measured the single-pixel sensitivity, which is defined here as the total Fisher information in the outgoing state for phase variations on each individual pixel on the hidden SLM. These measurements are performed by successively varying the phase shift induced by individual pixels sequentially, instead of varying the phase shift induced by the cross-shaped target as a whole (Methods). We find that the maximum information state is primarily sensitive to a few pixels in the centre of the cross (Fig. 2d), which confirms its economical wavefunction design. We emphasize that optimal states are not conceived to reveal the shape of the target, but to estimate the phase shift it induces. This does not require the intensity to be uniformly distributed on the area defining the target, explaining why its shape is not always fully revealed.

An important characteristic of maximum information states is their specificity with respect to both the position of the observer and to the observable of interest. To explicitly probe the influence of the observer, we repeated the experiment from above, but instead with a reduced field of view in the detection plane (Fig. 2e–h and Extended Data Fig. 2). The maximum information state readjusts to this new observer by redirecting the spatial distributions of its outgoing signal intensity (Fig. 2f) and of its Fisher information per unit area (Fig. 2g) straight to the selected observer area. This confirms the essential role played by the set of optical modes we incorporate into the definition of maximum information states. Although the single-pixel sensitivity (Fig. 2h) is similar to that observed when the whole field of view is taken into account (compare with Fig. 2d), it is here more uniformly distributed inside the cross-shaped area. Such a redistribution in the plane of the hidden SLM is associated with smaller diffraction angles, thus allowing for a reduced spatial extent of the intensity distribution in the plane of the diffuser. To demonstrate the specificity of maximum information states with respect to the observable of interest, we also repeated the experimental procedure by choosing the horizontal position x of a circular phase object (radius 30 µm) as being the observable parameter of interest

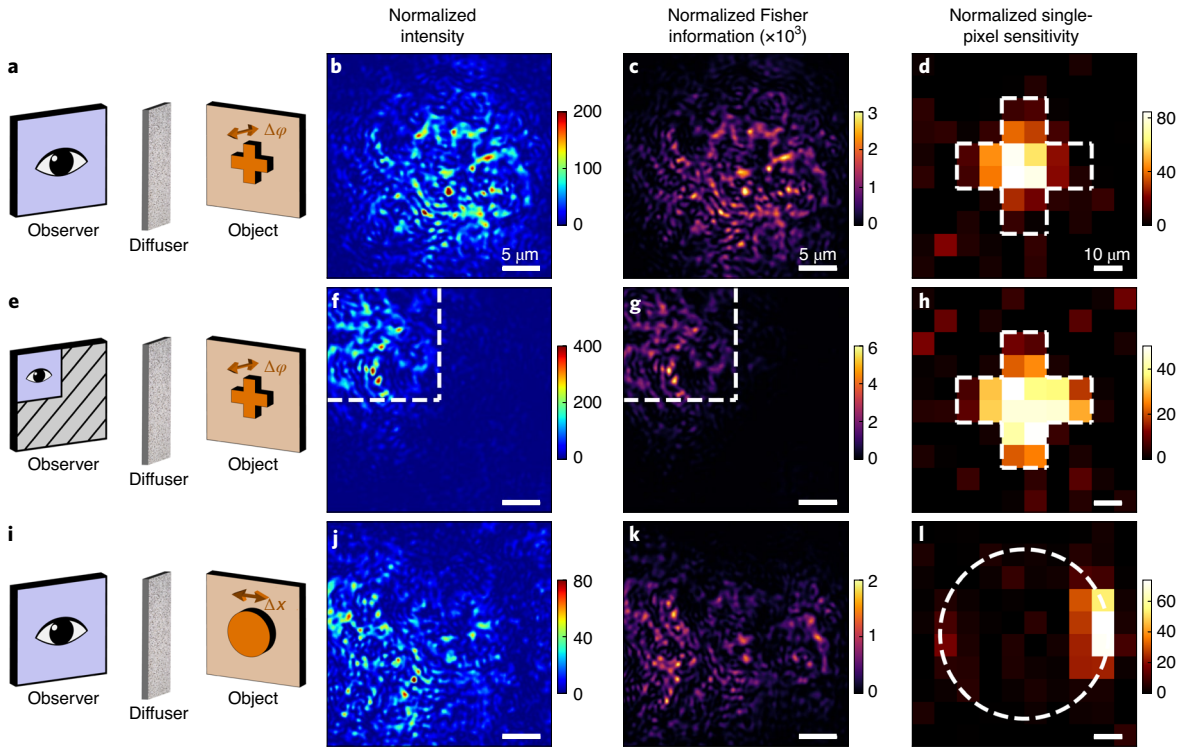

Fig. 2 | Characteristics of maximum information states. a, Sketch of the experiment: the observer (left) is a camera with a field of view covering 880 μm², separated by a diffuser (middle) from a cross-shaped target object (right) that induces a phase shift φ as our observable parameter of interest. **b**,**c**, Measured spatial distributions of the intensity (**b**) and of the Fisher information per unit area (**c**) for the optimal state with maximum overall information content, normalized by the average signal intensity and by the average Fisher information per unit area under plane wave illumination, respectively. **d**, Single-pixel sensitivity measured by shifting the phase of each pixel in the target area of the hidden SLM for the optimal state, normalized by the average single-pixel sensitivity under plane wave illumination. The cross-shaped target is indicated by white dashed lines. **e**–**h**, Analogous to **a**–**d** when the field of view of the camera covers a reduced area of 220 μm², as delimited by white dashed lines in **f** and **g**. The maximum information state fully adjusts to the changes in the observer by delivering the Fisher information here primarily to the limited field of view. **i**–**l**, Analogous to **a**–**d** when the observable parameter is the horizontal position x of a circular phase object. The maximum information state adapts to the change in observable by redirecting its incoming intensity to those pixels on the very right or left edges of the target object that are most strongly affected by a lateral displacement Δx.

(Fig. 2i–l and Extended Data Fig. 3). The single-pixel sensitivity is now localized on the right or left edge of the object, which attests that maximum information states selectively focus light waves onto those specific areas of the object that have the most pronounced dependence on the observable of interest. The maximum information state typically focuses on a single edge rather than on both edges simultaneously, which is to be expected as the mirror symmetry in the system is broken by the diffuser.

To exemplify the advantages that these features provide for measurements with very few photons where the estimation precision is limited by shot noise, we reduced the incident photon flux by placing a neutral density filter (fractional transmittance 8.3×10^{-7}) in the optical path. Under these conditions, illuminating the medium with a plane wave does not allow reliable estimations of the phase shift induced by target. This is confirmed by calculating the precision limit σ_{CRB} for the 2,437 plane waves used to construct the reflection matrix (Supplementary Section 2.1). For these plane waves, the median of the obtained phase distribution is 1.8 rad, with a minimum value of 0.60 rad (Fig. 3a). In contrast, the precision limit associated with the maximum information state equals 0.066 rad, an entire order of magnitude smaller than the minimum value measured for plane waves. Whereas reaching this precision limit would require amplitude and phase modulation of the incident field, we modulate only its phase via the input SLM in the experiments. We find that the precision limit associated with phase-only modulation of the maximum information state equals 0.078 rad, a value that is only slightly larger than that for a joint amplitude and phase modulation. This observation corroborates the robustness of our approach with respect to small errors or imperfections in the preparation of the incident state.

To demonstrate the practical implementation of the estimation process with a maximum information state, we used this state to illuminate the medium and performed a sequence of measurements. The observable parameter we estimate is φ (the phase shift induced by the cross-shaped target), which is varied every 20 measurements between −0.25 rad and 0.25 rad in a step-like manner. From the knowledge of the expected outgoing state and its derivative with respect to φ, we can construct the minimum-variance unbiased estimator of φ applicable to small parameter variations (Supplementary Section 2.2). We can then estimate the value of φ from measurements of the outgoing state (Extended Data Fig. 4). Despite only approximately 24,000 incident photons probing the medium per measurement, each step can be clearly resolved (Fig. 3b,c). The observed standard error on the estimates is 0.11 rad, which corresponds to a transverse displacement of the target of 9.6 nm (see Extended Data Fig. 5 for estimations of lateral displacements). The observed standard error on the estimates almost reaches the precision limit predicted by the Cramér–Rao inequality. This confirms that shot noise is the dominant source of noise in our experiment, and demonstrates that the precision limit is correctly predicted from

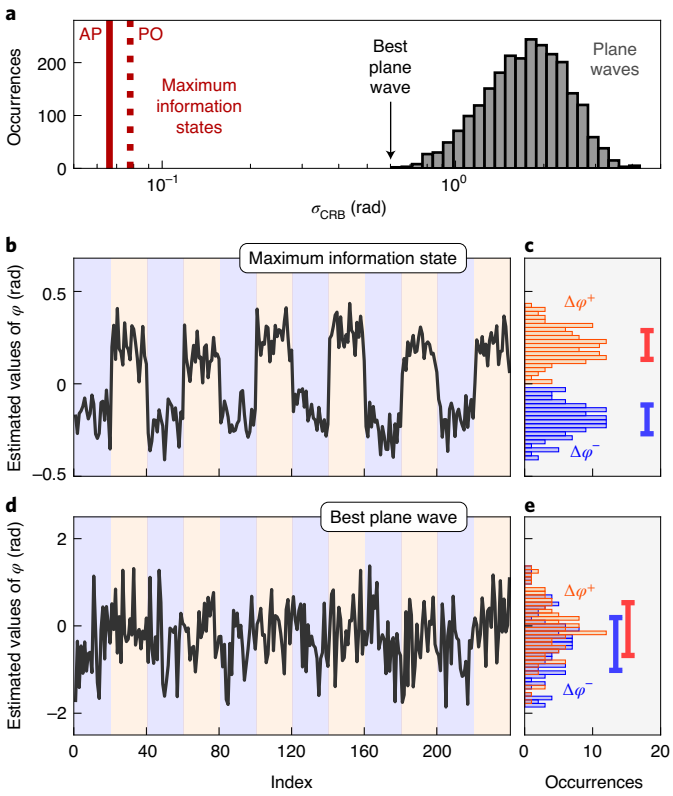

Fig. 3 | Demonstration of optimal estimations. a, Histogram of precision limits for the 2,437 plane waves used to construct the reflection matrix (the observable parameter is φ of the cross-shaped target shown in Fig. 2a). Compared with the best plane wave, the precision limit is improved by an order of magnitude with maximum information states (AP, amplitude and phase modulation; PO, phase-only modulation). **b**, Estimated phase shift of the cross-shaped target as a function of measurement index for measurements performed by illuminating the medium with the maximum information state. The red and blue shading indicates the sign of φ. **c**, Histograms of estimated angles for a positive phase shift ($\Delta\varphi^+ = +0.25$ rad) and a negative phase shift ($\Delta\varphi^- = -0.25$ rad) applied by the hidden SLM. The error bars represent $2\sigma_{CRB}$. **d**,**e**, Analogous to **b** and **c** for measurements performed by illuminating the medium with the best plane wave.

reflection matrix measurements. We applied the same procedure for measurements performed by illuminating the medium with the best plane wave used to construct the reflection matrix. The precision limit is then much larger than the step size, thereby prohibiting a clear detection of the phase steps (Fig. 3d,e).

The operator F_θ used in our analysis not only constitutes an operational tool for the identification of maximum information states, but is also deeply connected to fundamental concepts in optics. Provided that reciprocity holds in terms of the transposition symmetry of the scattering matrix ($S^T = S$), we can show (Supplementary Section 1.5) that the iterative phase conjugation of a small perturbation $\Delta\theta$ converges towards the largest eigenvalues of F_θ. This insight not only suggests a potentially useful approach to identify maximum information states, but also provides a new understanding of existing focusing procedures based on time-reversed adapted perturbation[20–22]. Moreover, in the ideal case of a unitary S matrix ($S^\dagger = S^{-1}$) where all optical modes supported by the system are accessible, we obtain the identity $F_\theta = Q_\theta^2$, where $Q_\theta = -iS^{-1}\partial_\theta S$ is the generalized Wigner–Smith operator. This operator was recently introduced to design optimal light fields for optical micromanipulation in complex media[15,16]. The simple relation between F_θ and Q_θ suggests a new interpretation of Q_θ as the operator representing the measurement backaction on the conjugate quantity to θ. The eigenstates of Q_θ (also called principal modes) have the remarkable property of being insensitive with respect to small variations in θ except for a global phase factor[23,24]. Likewise, the Fisher information of maximum information states is exclusively enclosed in variations of the global phase of the outgoing state, rather than in the state's intensity variations or speckle decorrelation. Nevertheless, this property strictly holds only for a unitary S matrix and deviations from this property are observed in our experiments (Supplementary Section 3.3). It is also interesting to discuss the special case for which the observable of interest is the dielectric constant ϵ of a target. Provided that $S^\dagger = S^{-1}$, eigenstates of Q_ϵ maximize the integrated intensity inside the target[16], which implies that maximum information states are then, at the same time, the light states that maximize power delivery to the target. Finally, although we have considered a scalar parameter θ in our analysis, our formalism also enables the identification of light states that maximize the trace of the multiparameter Fisher information matrix (Supplementary Section 1.6), thus providing a possible strategy with which to perform precise estimations of multiple parameters.

To summarize, we demonstrate a method to identify and produce coherent light fields that are optimal for precision measurements in a complex environment. This work opens up new perspectives to enhance the performance of imaging techniques[13] and, by simultaneously engineering the Fisher information operator itself, could also be used to improve the sensitivity of existing nanostructured sensing devices[25,26]. We emphasize that our results are generally applicable to any parametric dependence of a wave field and can thus be transferred to other types of waves, such as in acoustics[27] or in the microwave regime[28]. Finally, it can be expected that the bound derived in this work for coherent states will be surpassed using quantum metrology protocols[11,29,30]. In this context, our results provide a general benchmark with which to assess the performance of quantum states optimized for parameter estimation, and suggest a new path towards the identification of optimally-sensitive quantum states of light using scattering matrices of complex systems.

Online content

Any methods, additional references, Nature Research reporting summaries, source data, extended data, supplementary information, acknowledgements, peer review information; details of author contributions and competing interests; and statements of data and code availability are available at https://doi.org/10.1038/s41567-020-01137-4.

Received: 17 July 2020; Accepted: 1 December 2020;
Published online: 21 January 2021

References

1. Park, Y., Depeursinge, C. & Popescu, G. Quantitative phase imaging in biomedicine. *Nat. Photon.* **12**, 578–589 (2018).
2. Taylor, R. W. & Sandoghdar, V. Interferometric scattering microscopy: seeing single nanoparticles and molecules via Rayleigh scattering. *Nano Lett.* **19**, 4827–4835 (2019).
3. Osten, W. & Reingand, N. *Optical Imaging and Metrology: Advanced Technologies* (John Wiley & Sons, 2012).
4. van Putten, E. G., Lagendijk, A. & Mosk, A. P. Nonimaging speckle interferometry for high-speed nanometer-scale position detection. *Opt. Lett.* **37**, 1070–1072 (2012).
5. Shechtman, Y., Sahl, S. J., Backer, A. S. & Moerner, W. Optimal point spread function design for 3D imaging. *Phys. Rev. Lett.* **113**, 133902 (2014).
6. Balzarotti, F. et al. Nanometer resolution imaging and tracking of fluorescent molecules with minimal photon fluxes. *Science* **355**, 606–612 (2017).
7. Ambichl, P. et al. Super- and anti-principal-modes in multimode waveguides. *Phys. Rev. X* **7**, 041053 (2017).
8. Yuan, G. H. & Zheludev, N. I. Detecting nanometric displacements with optical ruler metrology. *Science* **364**, 771–775 (2019).

9. Juffmann, T., de los Ríos Sommer, A. & Gigan, S. Local optimization of wave-fronts for optimal sensitivity phase imaging (LowPhi). *Opt. Commun.* **454**, 124484 (2020).
10. Bouchet, D., Carminati, R. & Mosk, A. P. Influence of the local scattering environment on the localization precision of single particles. *Phys. Rev. Lett.* **124**, 133903 (2020).
11. Giovannetti, V., Lloyd, S. & Maccone, L. Advances in quantum metrology. *Nat. Photon.* **5**, 222–229 (2011).
12. Rotter, S. & Gigan, S. Light fields in complex media: mesoscopic scattering meets wave control. *Rev. Mod. Phys.* **89**, 015005 (2017).
13. Barrett, H. H. & Myers, K. J. *Foundations of Image Science* (John Wiley & Sons, 2013).
14. Kay, S. *Fundamentals of Statistical Processing* Vol. I (Prentice Hall, 1993).
15. Ambichl, P. et al. Focusing inside disordered media with the generalized Wigner-Smith operator. *Phys. Rev. Lett.* **119**, 033903 (2017).
16. Horodynski, M. et al. Optimal wave fields for micromanipulation in complex scattering environments. *Nat. Photon.* **14**, 149–153 (2020).
17. Mosk, A. P., Lagendijk, A., Lerosey, G. & Fink, M. Controlling waves in space and time for imaging and focusing in complex media. *Nat. Photon.* **6**, 283–292 (2012).
18. Fang, P., Zhao, L. & Tian, C. Concentration-of-measure theory for structures and fluctuations of waves. *Phys. Rev. Lett.* **121**, 140603 (2018).
19. Braunstein, S. L., Caves, C. M. & Milburn, G. J. Generalized uncertainty relations: theory, examples, and Lorentz invariance. *Ann. Phys.* **247**, 135–173 (1996).
20. Zhou, E. H., Ruan, H., Yang, C. & Judkewitz, B. Focusing on moving targets through scattering samples. *Optica* **1**, 227–232 (2014).
21. Ma, C., Xu, X., Liu, Y. & Wang, L. V. Time-reversed adapted-perturbation (TRAP) optical focusing onto dynamic objects inside scattering media. *Nat. Photon.* **8**, 931–936 (2014).
22. Ruan, H. et al. Focusing light inside scattering media with magnetic-particle-guided wavefront shaping. *Optica* **4**, 1337–1343 (2017).
23. Carpenter, J., Eggleton, B. J. & Schröder, J. Observation of Eisenbud–Wigner–Smith states as principal modes in multimode fibre. *Nat. Photon.* **9**, 751–757 (2015).
24. Xiong, W. et al. Spatiotemporal control of light transmission through a multimode fiber with strong mode coupling. *Phys. Rev. Lett.* **117**, 053901 (2016).
25. Hodaei, H. et al. Enhanced sensitivity at higher-order exceptional points. *Nature* **548**, 187–191 (2017).
26. Chen, W., Kaya Özdemir, S., Zhao, G., Wiersig, J. & Yang, L. Exceptional points enhance sensing in an optical microcavity. *Nature* **548**, 192–196 (2017).
27. Gérardin, B., Laurent, J., Derode, A., Prada, C. & Aubry, A. Full transmission and reflection of waves propagating through a maze of disorder. *Phys. Rev. Lett.* **113**, 173901 (2014).
28. Shi, Z. & Genack, A. Z. Transmission eigenvalues and the bare conductance in the crossover to Anderson localization. *Phys. Rev. Lett.* **108**, 043901 (2012).
29. Giovannetti, V., Lloyd, S. & Maccone, L. Quantum metrology. *Phys. Rev. Lett.* **96**, 010401 (2006).
30. Fiderer, L. J., Fraïsse, J. M. & Braun, D. Maximal quantum Fisher information for mixed states. *Phys. Rev. Lett.* **123**, 250502 (2019).

Methods

Optical set-up. The light source used is a continuous-wave solid-state laser (Coherent OBIS 532-120 LS FP) emitting at 532 nm. The laser light was coupled to a single-mode polarization-maintaining fibre and out-coupled using a collimator (Schäfter+Kirchhoff, 60FC-L-4-M75-01). The beam was separated into a signal path and a reference path using a 50:50 beamsplitter. In the signal path, the light beam passed a 50:50 beamsplitter and was then modulated by the input SLM (Holoeye Pluto VIS). It could then pass different neutral density filters that were mechanically placed or removed. The incident power on the objective was: 36.1 µW when all density filters are removed from the optical path; 275 nW when a neutral density filter of optical density 2 (ND2) was placed in the optical path (measured fractional transmittance $\mathcal{T}' = 0.76\times10^{-2}$); and 30 pW when a neutral density filter of optical density 6 (ND6) was placed in the optical path (measured fractional transmittance $\mathcal{T} = 0.83\times10^{-6}$).

The surface of the SLM was imaged onto a ground glass diffuser using a 200 mm lens and a ×50 objective (Nikon 50X CFI60 TU Plan Epi ELWD, 0.6 NA). A 90:10 beamsplitter was located between the lens and the objective. The diffuser was made by polishing a microscope coverslip. The resulting scattering angle, defined from the full-width at half-maximum of the transmitted intensity distribution, was approximately 15°. The diffuser was mounted on the windows of the hidden SLM (Holoeye Pluto BB) at a distance of 1.2 mm. The surface of the diffuser was then imaged using the objective, a 200 mm lens and a charge-coupled device camera (AVT Stingray F145-B) with an exposure time of 300 µs. Camera acquisition was triggered by the input SLM to limit phase noise due to the flicker of the SLM. Before reaching the camera, the beam passed a polarizer to ensure that only the horizontal component of the field was measured, and also passed a 90:10 beamsplitter to recombine the reference path with the signal path. Both quadratures of the complex field were measured in a single shot using digital off-axis holography. Using a tilted beam instead of the optimally shaped reference field does not impact the shape of the incident field optimized for the estimation of φ, but leads to a reduction in the Fisher information by a factor of two (Supplementary Section 2.1).

Construction of the reflection matrix and its derivative. We constructed densely sampled reflection matrices relating incident field states to reflected ones[31,32]. Reflection matrix measurements were performed with no density filter in the signal path. To illuminate the medium, we varied the incidence angle of a Gaussian beam characterized by a full-width at half-maximum of 120 µm, which was four times larger than the field of view (such Gaussian beams are referred to as plane waves here). We probed $M = 2{,}437$ different incidence angles, covering a numerical aperture of 0.5. The sampling was performed using a triangular lattice (in Fourier space), with a lattice constant taken to be the smallest angular separation at which the complex inner product of nearest-neighbour fields drops to zero.

For each incident angle, we recorded the reflected field using digital off-axis holography[33,34]. This method relies on a reference beam that is tilted by an angle with respect to the reflected signal beam. The complex field is then numerically reconstructed from the measured holograms by digitally filtering the zero-order component. In our experiments, the reflected field was sampled using a triangular lattice, with a lattice constant that we determined by finding the distance between the maximum and the first minimum of the autocorrelation of a random field. We used $N = 2{,}465$ different sampling points, covering an area of 880 µm^2 on the surface of the diffuser. The reflection matrix r was therefore constructed column by column and, as a result, we obtained a $2{,}465\times2{,}437$ matrix. This matrix could then be used to faithfully predict the outgoing state for any incident state (Supplementary Section 3.1).

In the initial experiment, the parameter of interest was the phase shift φ generated by a cross-shaped target object. The reflection matrix r was then measured at an angle $\varphi = \varphi_0$ by setting the phase shift induced by all pixels of the hidden SLM to a given value. Note that φ_0 could be set to zero without loss of generality. To estimate the derivative of the reflection matrix with respect to φ, we measured two other reflection matrices $r(\varphi_0 - \Delta\varphi)$ and $r(\varphi_0 + \Delta\varphi)$, where $\Delta\varphi = 0.54$ rad. We could then estimate $\partial_\varphi r$ by applying the centred finite difference scheme $\partial_\varphi r \simeq [r(\varphi_0 + \Delta\varphi) - r(\varphi_0 - \Delta\varphi)]/(2\Delta\varphi)$. This matrix could then be used to faithfully predict the derivative of the outgoing state with respect to φ for any incident state (Supplementary Section 3.2).

In another experiment, the parameter of interest was chosen to be the lateral position x of a circular object. In this case, a super-Gaussian function of order 7 was displayed by the hidden SLM, with a full-width at half-maximum equal to 60 µm. The phase difference between the object and the background was set to $\pi/2$ rad and r was then measured at a position $x = x_0$. To estimate the derivative of the reflection matrix with respect to x, we measured two other reflection matrices $r(x_0 - \Delta x)$ and $r(x_0 + \Delta x)$, where $\Delta x = 5$ µm. We could then estimate $\partial_x r$ by applying the centred finite difference scheme $\partial_\varphi r \simeq [r(x_0 + \Delta x) - r(x_0 - \Delta x)]/(2\Delta x)$.

Measurement of the single-pixel sensitivity. To measure the single-pixel sensitivity, we successively varied the phase shift φ_j induced by each individual pixel j for 100 pixels covering an area of 6,400 µm^2 on the surface of the hidden SLM. This allowed us to access the derivative of the outgoing field with respect to φ_j using a centred difference scheme, and to calculate the associated Fisher information using equation (1). For each individual pixel, we performed an averaging of the derivative of the outgoing field over ten independent measurements. Once the Fisher information was calculated, we also subtracted a residual noise floor that we estimated by taking different measurements of the same outgoing state. We performed the same analysis by illuminating the medium with the maximum information state and with different plane waves, and we normalized the values obtained for the maximum information state using the average value obtained with different plane waves. Note that a high single-pixel sensitivity cannot be achieved without a high intensity inside the pixel area. Thus, mapping the single-pixel sensitivity in the plane of the hidden SLM also provided us with an indirect way to approximate the intensity distribution in the plane of the hidden SLM.

Monitoring of the global phase drift. Owing to the long acquisition time (113 min in total), the global phase of the measured outgoing field slowly drifted in time because of the imperfect thermal stability of the experimental set-up. During the acquisition, we continuously monitored this drift by regularly measuring a known outgoing field as a phase reference[32]. We used different phase-reference fields depending on the incident power on the sample.

When no density filters were placed in the optical path, the phase-reference field was generated by illuminating the medium with a given plane wave, with a slight angle so that no reflection from the back-focal plane of the objective could be observed. We then calculated how the global phase of this field changed over time by using a complex inner product of the phase-reference field measured at a given time with the phase-reference field measured at the beginning of the acquisition.

When any density filter was placed in the optical path, we first calculated a truncated reflection matrix r', which did not include the few columns for which reflection from the back-focal plane of the objective could be observed. The phase-reference field was generated by illuminating the medium using the right-singular vector of r' associated with its largest singular value. By doing so, we maximized the signal-to-noise ratio of phase-reference measurements. We then calculated how the global phase of this field changed over time by using a complex inner product of the phase-reference field measured at a given time with the field predicted from the knowledge of the reflection matrix.

Finally, we performed linear interpolations to estimate the global phase drift at any time during the acquisition, and we subsequently applied the appropriate phase correction to any measured data.

Data availability

Source data are provided with this paper. All other data that support the plots within this paper and other findings of this study are available from the corresponding author on reasonable request.

References

31. Popoff, S. M. et al. Measuring the transmission matrix in optics: an approach to the study and control of light propagation in disordered media. *Phys. Rev. Lett.* **104**, 100601 (2010).
32. Pai, P., Bosch, J. & Mosk, A. P. Optical transmission matrix measurement sampled on a dense hexagonal lattice. *OSA Contin.* **3**, 637–648 (2020).
33. Takeda, M., Ina, H. & Kobayashi, S. Fourier-transform method of fringe-pattern analysis for computer-based topography and interferometry. *J. Opt. Soc. Am.* **72**, 156–160 (1982).
34. Cuche, E., Marquet, P. & Depeursinge, C. Spatial filtering for zero-order and twin-image elimination in digital off-axis holography. *Appl. Opt.* **39**, 4070–4075 (2000).

Acknowledgements

We thank M. van Beurden, J. Bosch, S. Faez, M. Horodynski, M. Kühmayer, P. Pai and J. Seifert for insightful discussions and P. Jurrius, D. Killian and C. de Kok for technical support. This work was supported by the Netherlands Organization for Scientific Research NWO (Vici grant number 68047618 and Perspective project number P16-08) and by the Austrian Science Fund (FWF) under project number P32300 (WAVELAND).

Author contributions

D.B. and A.P.M. initiated the project. D.B. performed the experiments. D.B., S.R. and A.P.M. developed the concept, analysed the results and wrote the manuscript.

Competing interests

The authors declare no competing interests.

Additional information

Extended data is available for this paper at https://doi.org/10.1038/s41567-020-01137-4.

Supplementary information is available for this paper at https://doi.org/10.1038/s41567-020-01137-4.

Correspondence and requests for materials should be addressed to D.B.

Peer review information *Nature Physics* thanks Sébastien Popoff and Chushun Tian for their contribution to the peer review of this work.

Reprints and permissions information is available at www.nature.com/reprints.

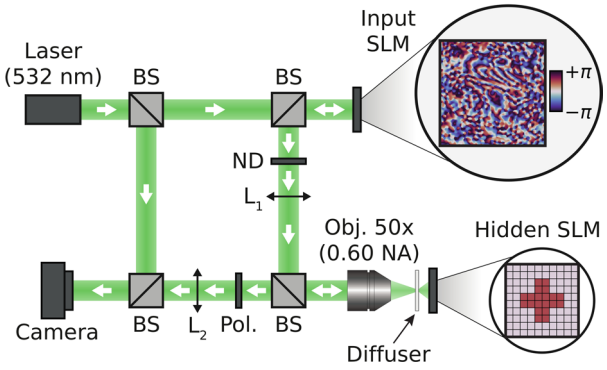

Extended Data Fig. 1 | Optical setup. The phases on the input SLM are modulated to reproduce the maximum information state, which reaches optimal sensitivity in its output with respect to any specified parameter characterizing the object displayed on the hidden SLM, such as phase variations or lateral displacements. Neutral density filters are removed for reflection matrix measurements. BS, beamsplitter; ND, neutral density filters; Obj, objective; NA, numerical aperture; Pol, linear polarizer; L_1 and L_2, lenses with focal length 200 mm.

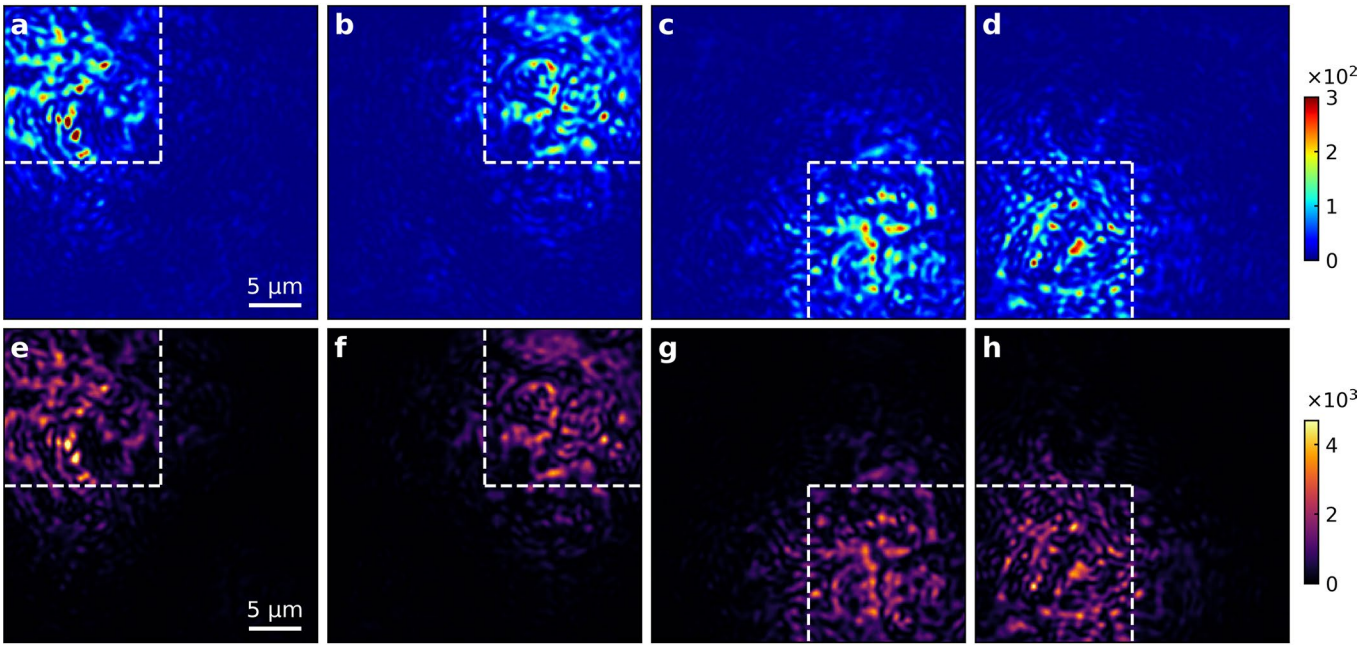

Extended Data Fig. 2 | Measured intensity and Fisher information distributions for maximum information states associated with different detection areas. a-d, Measured spatial distributions of the intensity for optimal states, normalized by the average signal intensity under plane wave illumination. The observable parameter is the phase shift induced by the cross-shaped target, and optimal states are defined here with respect to a reduced field of view of the camera that covers an area of 220 μm^2, as delimited by white dashed lines. **e-h**, Analogous to **a-d** for the measured spatial distribution of the Fisher information per unit area. Remarkably, the maximum information state always delivers the Fisher information to the designated observer window.

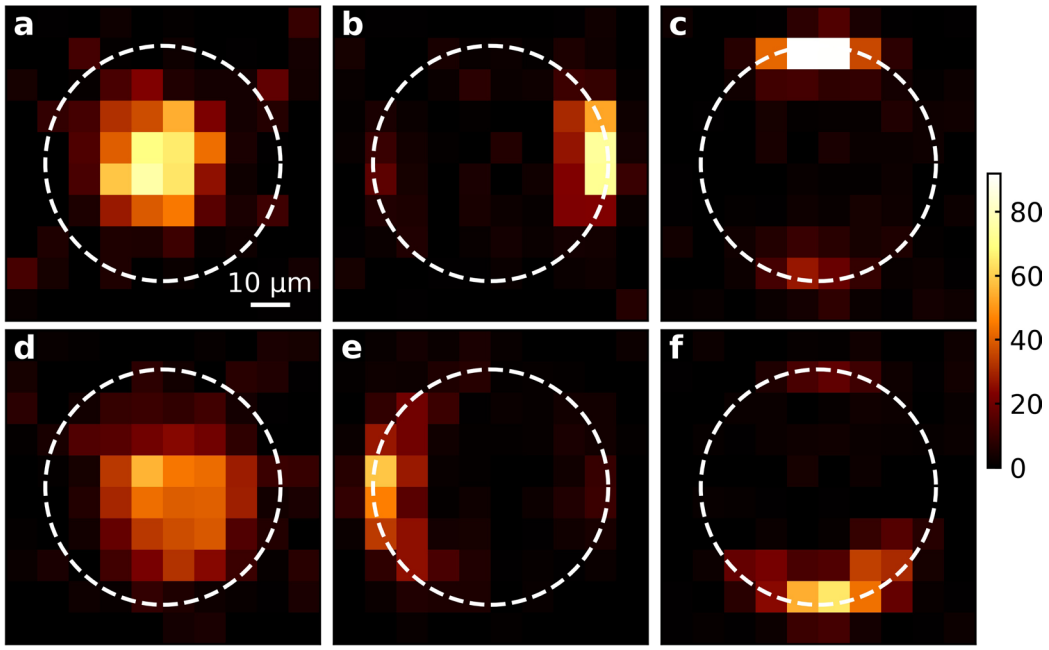

Extended Data Fig. 3 | Single-pixel sensitivity for maximum information states associated with different observable parameters. a-c, Single-pixel sensitivity measured by shifting the phase of each pixel in the target area of the hidden SLM for the optimal state, normalized by the average single-pixel sensitivity under plane-wave illumination. The object displayed on the hidden SLM is a circular phase object, whose position is delimited by a white dashed circle. The field of view of the detection camera covers here an area of 880 μm^2. The incident states used to illuminate the scattering medium are the maximum information states relative to a phase shift (**a**), a horizontal shift (**b**) and a vertical shift (**c**) of the object. **d-f**, Analogous to **a-c** when the field of view of the camera covers a reduced area of 144 μm^2. In all cases, the maximum information state directs the incoming intensity to those parts on the hidden SLM that are most affected by the change in the observable parameter. Interestingly, when the target parameter is either a horizontal or a vertical shift of the object, the maximum information state typically focuses on a single edge rather than on both edges simultaneously, which is to be expected as the mirror symmetry in the system is broken by the diffuser.

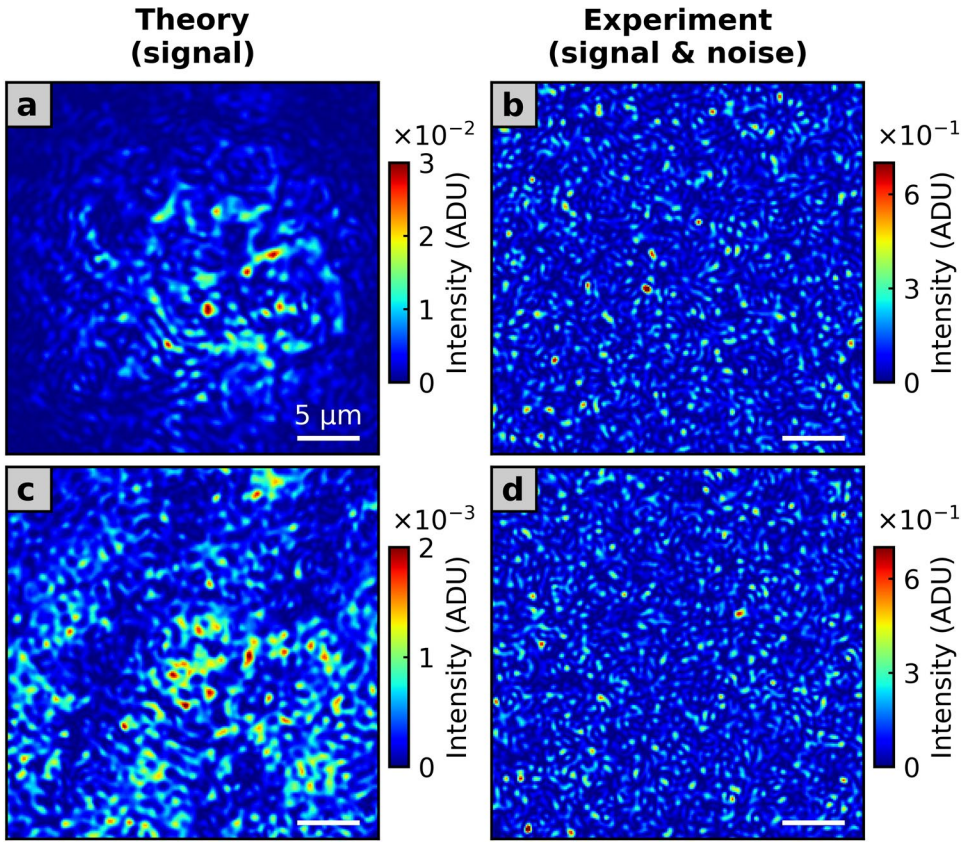

Extended Data Fig. 4 | Predicted and measured signal intensity distribution at low photon counts. a, Predicted distribution of the signal intensity for the optimal incident state expressed in analog-to-digital units (ADU). This distribution is calculated from the measured reflection matrix, considering that the neutral density filter ND6 (fractional transmittance 8.3×10^{-7}) is placed in the optical path. **b**, Measured distribution of the signal intensity for the optimal incident state when ND6 is in the signal path. Such measurements are shot-noise limited, and the observed signal-to-noise per pixel is largely smaller than unity. Thus, the measured distribution of the signal intensity appears as a random noise, which has been low-pass filtered by the data analysis procedure used to digitally reconstruct complex fields from off-axis intensity measurements. Despite this low signal-to-noise per pixel, such data allow to correctly estimate the phase shift induced by the hidden target when using the minimum variance unbiased estimator. This can be achieved since only a single parameter (the phase shift induced by the target) needs to be estimated from a large number of independent sampling points. The Fisher information associated with each pixel of the detection camera effectively adds up, resulting in a total Fisher information that is sufficient to resolve the phase steps induced on the hidden SLM. **c, d**, Analogous to **a** and **b** for the best plane wave used to construct the reflection matrix.

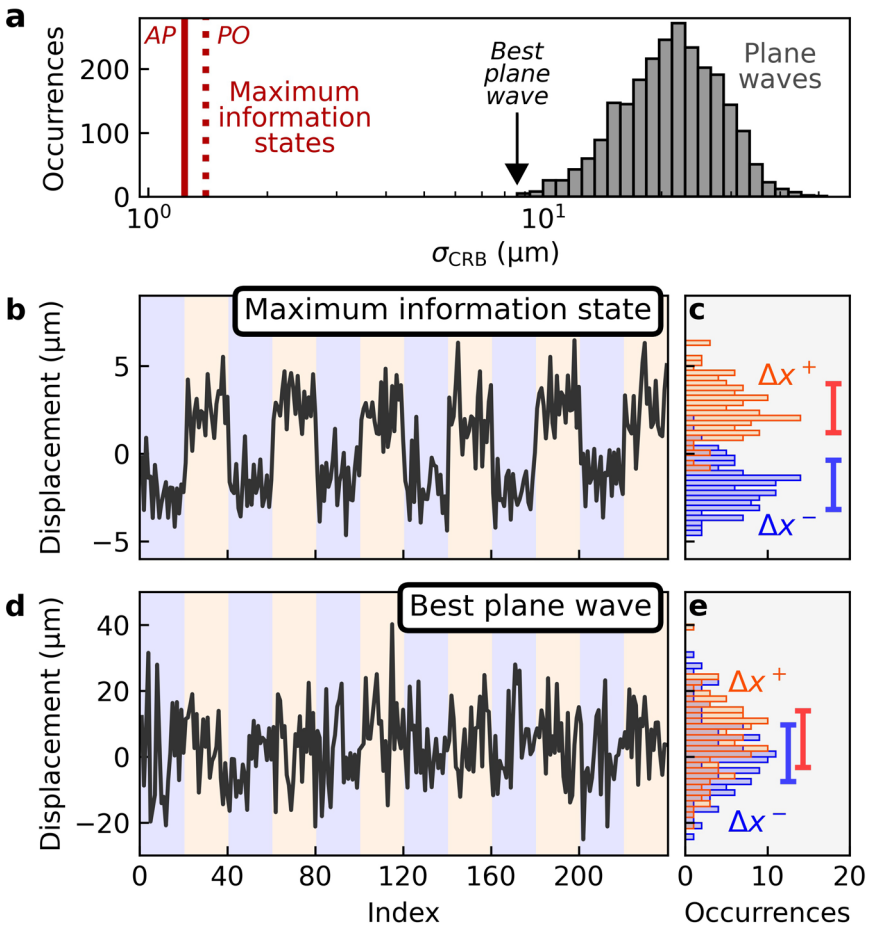

Extended Data Fig. 5 | Estimations of lateral displacements at low photon counts. Analogous to Fig. 3 when the observable parameter is the horizontal position x of the circular phase object shown in Fig. 2i. **a**, Histogram of precision limits for the 2,437 plane waves used to construct the reflection matrix and for the maximum information states (AP, amplitude and phase modulation; PO, phase-only modulation). **b**, Estimated lateral displacements of the circular phase object as a function of measurement index for measurements performed by illuminating the medium with the maximum information state. The calculated precision limit equals 1.4 μm, and the observed standard error on the estimates is 1.5 μm. **c**, Histograms of estimated angles for a positive lateral displacement ($\Delta x^+ = +2.5\ \mu$m) and a negative lateral displacement ($\Delta x^- = -2.5\ \mu$m) applied by the hidden SLM. The length of error bars equals 2 σ_{CRB}. **d, e**, Analogous to **b** and **c** for measurements performed by illuminating the medium with the best plane wave.